Supporting Information

Mechanochemical Adhesion and Plasticity in Multi-fiber Hydrogel Networks

Matthew D. Davidson, Ehsan Ban, Anna C.M. Schoonen, Mu-Huan Lee, Matteo D'Este, Vivek B. Shenoy, and Jason A. Burdick*

Experimental Section

Material Synthesis:

NorHA Synthesis: All materials were purchased from Sigma Aldrich unless noted. Two NorHA precursor macromers were synthesized for making NorHA-Hyd or NorHA-Ald. Specifically, NorHA-Hyd was made by coupling hydrazide groups to NorHA that was initially synthesized from medium molecular weight HA (~76 kDa), while NorHA-Ald was synthesized by oxidizing NorHA that was initially synthesized with high molecular weight HA (~250 kDa). To solubilize HA in DMSO, sodium HA (Lifecore) was dissolved in DI H_2O at 2 wt % with Dowex® resin (50Wx8 ion-change resin) at a ratio of 3:1 (resin: HA by weight) and mixed for at least 30 minutes. Resin was filtered, the filtrate was titrated to pH 7.03 with diluted tetrabutylammonium hydroxide (TBA-OH) and then frozen and lyophilized. TBA modification of HA was confirmed with NMR. HA-TBA was dissolved in anhydrous DMSO at 2 wt% with 4-(dimethylamino)pyridine (DMAP) (1.5 molar ratio to HA-TBA repeat units) and 5-norbornene-2-carboxylic acid (3:1 molar ratio to HA-TBA repeat units) under an N_2 atmosphere. Once fully dissolved, di-tert-butyl decarbonate (Boc_2O, 0.4 M ratio to HA-TBA units) was injected into the vessel and the reaction was carried out for ~20 hrs at 45 °C. The reaction was quenched with 2X cold (4°C) DI H_2O and dialyzed against water with 0.25g NaCl/ L of DI H_2O for 3 days. NorHA was then mixed with NaCl (1g NaCl/ 100ml solution) and precipitated in ice cold acetone (1L acetone/100ml solution). The precipitate was re-dissolved in DI H_2O, dialyzed for 5 days, frozen and lyophilized. Norbornene functionalization was confirmed with ^1H NMR (**Figure S1**).

NorHA-Hydrazide Synthesis: NorHA-hydrazide was synthesized by dissolving NorHA at 2 wt% in DI H_2O with adipic acid dihydrazide (13g/g of HA). 1-ethyl-3-(3-dimethylaminopropyl)carbodiimide (EDC, 10mM) and hydroxybezotriazole (HOBT, 10mM) were dissolved separately in a solution of DMSO:water (1:1) and added to the reaction vessel dropwise. pH was adjusted to 6.8 with HCl initially and every 30 minutes for four hours, and then the reaction proceeded overnight at room temperature. NorHA-Hyd was then dialyzed against DI H_2O for 3 days, precipitated using the same procedure carried out for NorHA above, dialyzed again for 5 days, frozen and lyophilized. Hydrazide modification of NorHA was confirmed with ^1H NMR (**Figure S1**).

NorHA-Aldehyde Synthesis: NorHA-aldehyde was synthesized by dissolving HWM NorHA at 1 wt% in DI H_2O with sodium periodate (1:4 or 1:8 periodate:HA molar ratio). The reaction was carried out for 2 hours protected from light at room temperature and quenched with 2 ml of ethylene glycol. The solution was dialyzed for 5 days against DI H_2O, frozen, and lyophilized. Modification of NorHA with aldehydes was confirmed with an aldehyde quantification assay (Abcam, ab138882) and Carbon-13 NMR (**Figure S2**).

Peptide Synthesis: Fluorescent RGD peptides (RhodamineB-GYGRGDSCG, 1436 g mol^{-1}) were synthesized with a thiol to allow for thiol-ene conjugation to NorHA, similarly to how RGD is conjugated for cell culture studies, and a fluorophore to permit visualization of the amount of peptide that was conjugated. Peptides were synthesized using solid state methods, as previously described.[14] Peptides were cleaved from resin in trifluoracetic acid, and precipitated in ether prior to lyophilization and storage at -20°C.

Electrospinning:

A 3.5 wt% (NorHA, NorHA-Ald, or NorHA-Hyd), 2.5 wt% PEO (900 kDa), 0.05 (v/v) % Irgacure 2959, 4 mg/ml fluorescent dextran (rhodamine-dextran or FITC-dextran, 70 kDa), were mixed with a 0.1 stoichiometric ratio of dithiothreitol (DTT) to norbornene groups (i.e. 0.1 thiols:norbornenes) in DDI H_2O, mixed at 250 rpm for 24 hours protected from light and loaded into syringes for electrospinning. To simultaneously electrospin 2 polymers, electrospinning jets were positioned on opposite sides of the electrospinning mandrel (**Figure S3**), while maintaining the same needle to collector distance (19 cm), flow rate (0.7 ml/hr), and voltage (+28-30 kV). Electrospinning was carried out in a custom humidity-controlled chamber (15-30% humidity) with a rotating mandrel (-5kV, ~350 RPM), deflectors (+4 kV) and needle gauge of 18.

Cell culture and staining:

Electrospun fibers were sterilized with germicidal UV for 1 hour, hydrated in DPBS, and conjugated with adhesive RGD peptides (sequence: GCGYG*RGD*SPG, GenScript). Fibrous hydrogels were incubated in a solution of 1mM thiolated-RGD, 0.05 (v/v) % I2959, and DPBS and RGD was conjugated to norbornene groups on HA using a photoinitiated thiol-ene reaction (5mw/cm^2 UV, 5 minutes). Fibers were washed 3 times with DPBS before cell seeding. Human mesenchymal stem cells (Lonza), passage 3, were cultured in alphaMEM (Gibco) supplemented with 10% FBS and 1% penicillin/streptomycin solution (Gibco). Cells were trypsinized with 0.05% Trypsin EDTA (Gibco) and seeded at 1.5x10^5 cells/ml directly onto the fibrous hydrogel networks, with a total volume of 1 ml. Cells were cultured on scaffolds, fixed with 4% formalin, actin and DNA were labeled with Alexa Flour 647 phalloidin (Thermo Fischer) and hoechst 33342, respectively.

Fiber network model:

To model the inelastic realignment of fibers after unloading of the fibrous matrices, we employed a discrete fiber network model.[1] Random networks were generated by the deposition of two different types of fibers in a planar domain. The position and orientation of the initially straight fibers were sampled from uniform probability distributions. The intersection points of the fibers were identified as crosslinks that modeled the initial junctions between the deposited fibers. These crosslinks constrained the relative motion and rotation of the two connected fibers and were modeled as rigid connections. Adhesions were also formed when fibers of different types came close during the deformation of the networks. [2]. Individual fibers were modeled using elastic beams with circular cross-sections of diameters 0.5 μm and 0.8 μm for the hydrazide and aldehyde fibers, respectively. The finite element simulations were performed using beams with reduced integration [3] and an implicit solution method [4]. Displacement-controlled tests were conducted by prescribing nodal displacements at the network boundaries in the direction of loading while allowing free network contractions in the transverse direction. The finite element model was updated after the addition or removal of elements, which modeled the new adhesions, and elastodynamic(inertial) effects were not considered in the simulations. Finite element calculations were performed using the ABAQUS software package. [5]

Continuum model:

A coarse-grained model of the deformation of the networks was developed using an inelastic constitutive law. This model represented the inelastic deformation of the network at the scale of the whole sample. At the time t, the state of deformation was described by the deformation gradient, $\boldsymbol{F}(t) = \nabla_{\boldsymbol{X}}\boldsymbol{x}$, where $\boldsymbol{X}$ and $\boldsymbol{x}$ denote the coordinates of the material particles at times 0 and t, respectively. The strain energy density required to deform the network by $\boldsymbol{F}(t)$ was denoted by W. The model accounts for both the preexisting crosslinks, representing the inter-fiber junctions and the crosslinks formed during deformation. As the network is stretched, it contracts in the direction transverse to loading. The previously distant fibers come close and form new adhesions. At the time τ, crosslinks form at the rate $\bar{k}_{on}$, and all previously formed crosslinks dissociate at the rate $\bar{k}_{off}\rho(\tau)$, where $\rho(\tau)$ is the density of crosslinks formed at the time τ. The deformation of each group of crosslinks was tracked with respect to the configuration where they were formed. The relative deformation gradient from time τ to time t was evaluated as

$$\boldsymbol{F}(\tau,t) = \boldsymbol{F}(t)\boldsymbol{F}(\tau)^{-1}. \tag{1}$$

The strain energy density of the network was

$$W = \int_0^t W^*\big(\boldsymbol{F}(\tau,t)\big)\dot{\rho}(\tau)d\tau. \tag{2}$$

W^* may be expressed as

$$W^* = W_b(\bar{I},J) + \sum_{i=1}^{3} f(\lambda_i), \tag{3}$$

where W_b is a neo-Hookean energy density, representing the unaligned fibers and f is an exponential function, expressing the strain-stiffening of the fibers re-aligned to the direction of maximum stretch during deformation.[6] W_b includes the parameters resembling bulk and shear moduli of 600 (kPa) and 300 (kPa), respectively, previously outlined in Ref. [6]. f was described by a fibrous stiffness of 300 (kPa), an exponent of stiffening of 2, and a threshold stretch of 1.01.[6]

The stretch dependent formation of crosslinks was modeled by a crosslink formation rate constant $\bar{k}_{on}$ equal to $\bar{k}_{on}^{0}\lambda$ for $\lambda < \lambda_{on}^{0}$, where $\bar{k}_{on}^{0}$ is the rate constant prior to deformation, and λ is the maximum principal stretch. λ_{on}^{0} is the threshold for the transition to a regime where the formation of crosslinks is accelerated by the highly deformed state of the network. After the threshold stretch, $\bar{k}_{on}$ was increased by $\bar{k}_{on}^{0}\beta_{on}(\lambda - \lambda_{on}^{0})$. β_{on} is a constant that tunes the activation of crosslink formation during deformation. Similarly, the rate constant of crosslink dissociation was expressed as $\bar{k}_{off}^{0}\lambda$ at $\lambda < \lambda_{off}^{0}$, where $\bar{k}_{off}^{0}$ and λ_{off}^{0} denote the rate constant for the dissociation of crosslinks in the absence of deformation and the threshold for the accelerated dissociation of crosslinks. For $\lambda > \lambda_{off}^{0}$, the rate of dissociation was increased by $\bar{k}_{off}^{0}\beta_{off}(\lambda - \lambda_{off}^{0})$, where β_{off} is a constant that tunes the increase of crosslink dissociation at large deformations. Two types of bonds were used to reproduce the experimentally observed stiffness of networks with and without holding during deformation. Prior to deformation, the rates of bond formation and dissociation were equal, leading to a density of crosslinks of $\bar{k}_{on}/\bar{k}_{off}$ for each type of bond.

Supplementary Table

Parameter	Value, type 1	Value, type 2
$\bar{k}_{off}^{0}$	2.38×10^{-5} s^{-1}	3.3×10^{-4} s^{-1}
$\bar{k}_{on}^{0}$	2.38×10^{-4} s^{-1}	5.5×10^{-6} s^{-1}
λ_{on}^{0}	1.4	1.49
λ_{off}^{0}	1.4	1.51
β_{on}	0.0	7×10^{5}
β_{off}	50.0	120.0

Table S1. Parameters that describe the formation and dissociation of crosslinks in the coarse-grained constitutive model.

Supplementary Figures

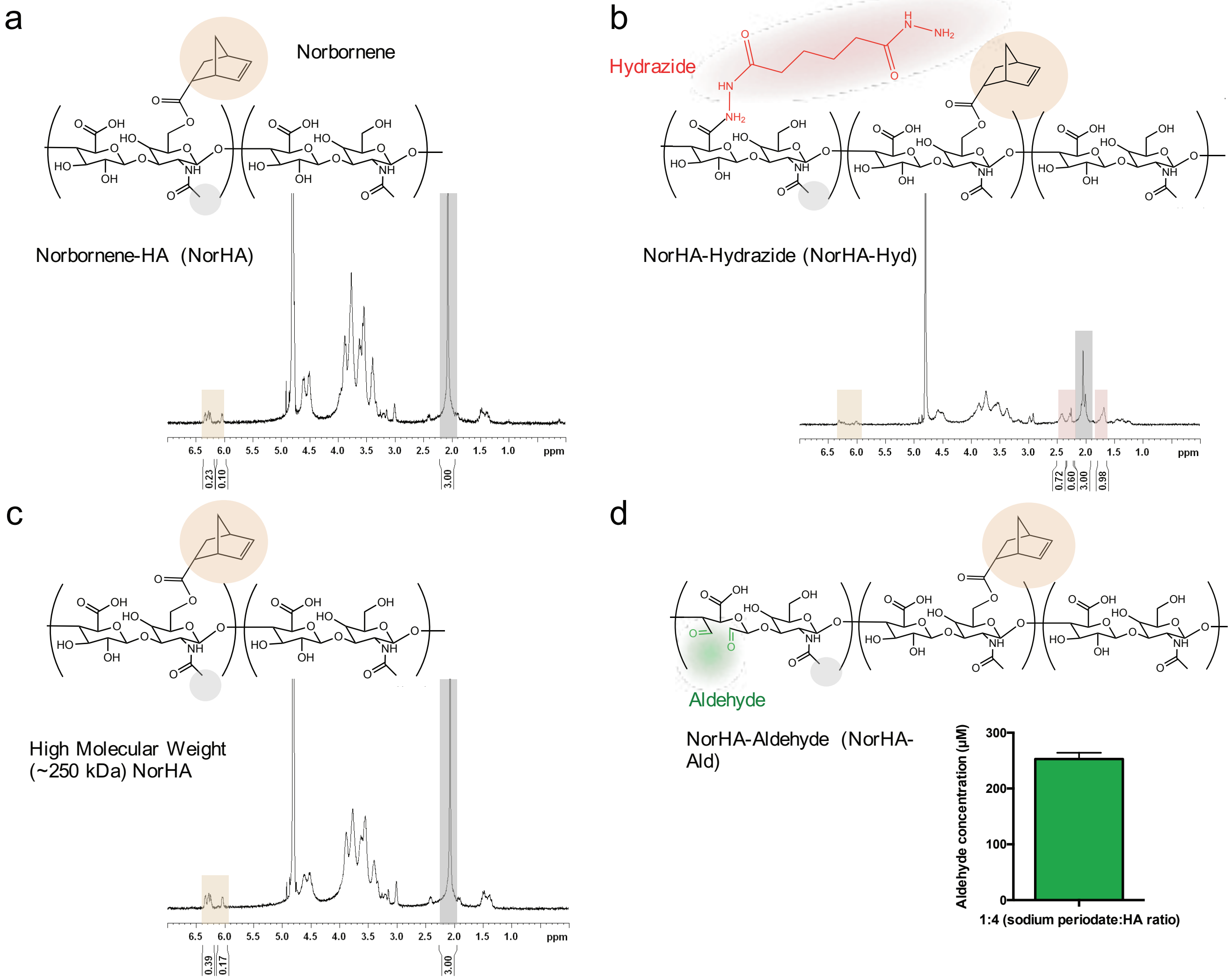

Figure S1. ^{1}H NMR characterization of modified HA and quantification of aldehyde modification. (a) Norbornene modification (~17%) of HA was determined by integration of the vinyl peaks (2H, shaded orange) relative to methyl group of HA (3H, shaded grey). (b) Hydrazide modification (~29%) of NorHA was determined by integration of the butyl linker (8H, shaded in red) relative to methyl group of HA (3H, shaded grey). (c) Norbornene modification (~33%) of high molecular weight HA was determined by integration of the vinyl peaks (2H, shaded orange) relative to methyl group of HA (3H, shaded grey). (d) Concentration of aldehydes in a 2 wt % solution of HA oxidized with increasing amounts of sodium periodate. A 1:4 (Sodium periodate:HA) ratio was used throughout this work as previously described.[7]

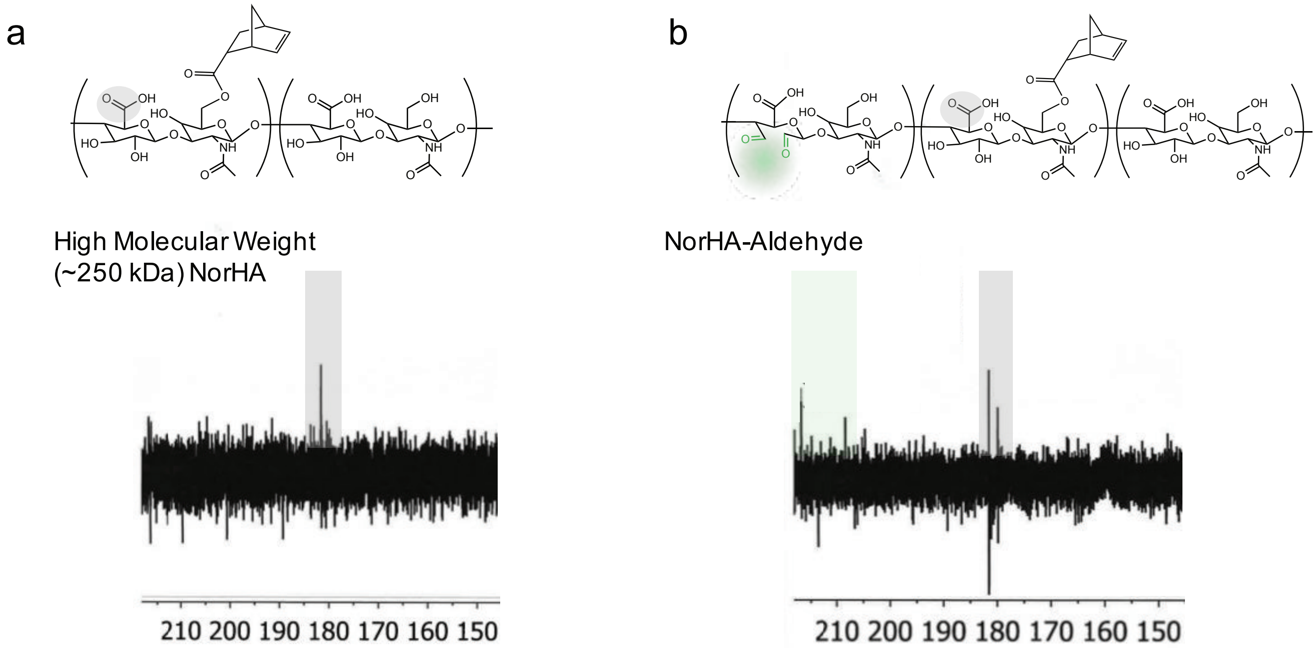

Figure S2. Carbon-13 NMR characterization of HA modified with norbornene and aldehyde groups. (a) Only β-D-glucoronic acid units of HA (~180, grey) were observed in norbornene modified HA (NorHA), while, (b) aldehyde modification of NorHA was confirmed with the appearance of carbonyl peaks (>200 ppm, green).

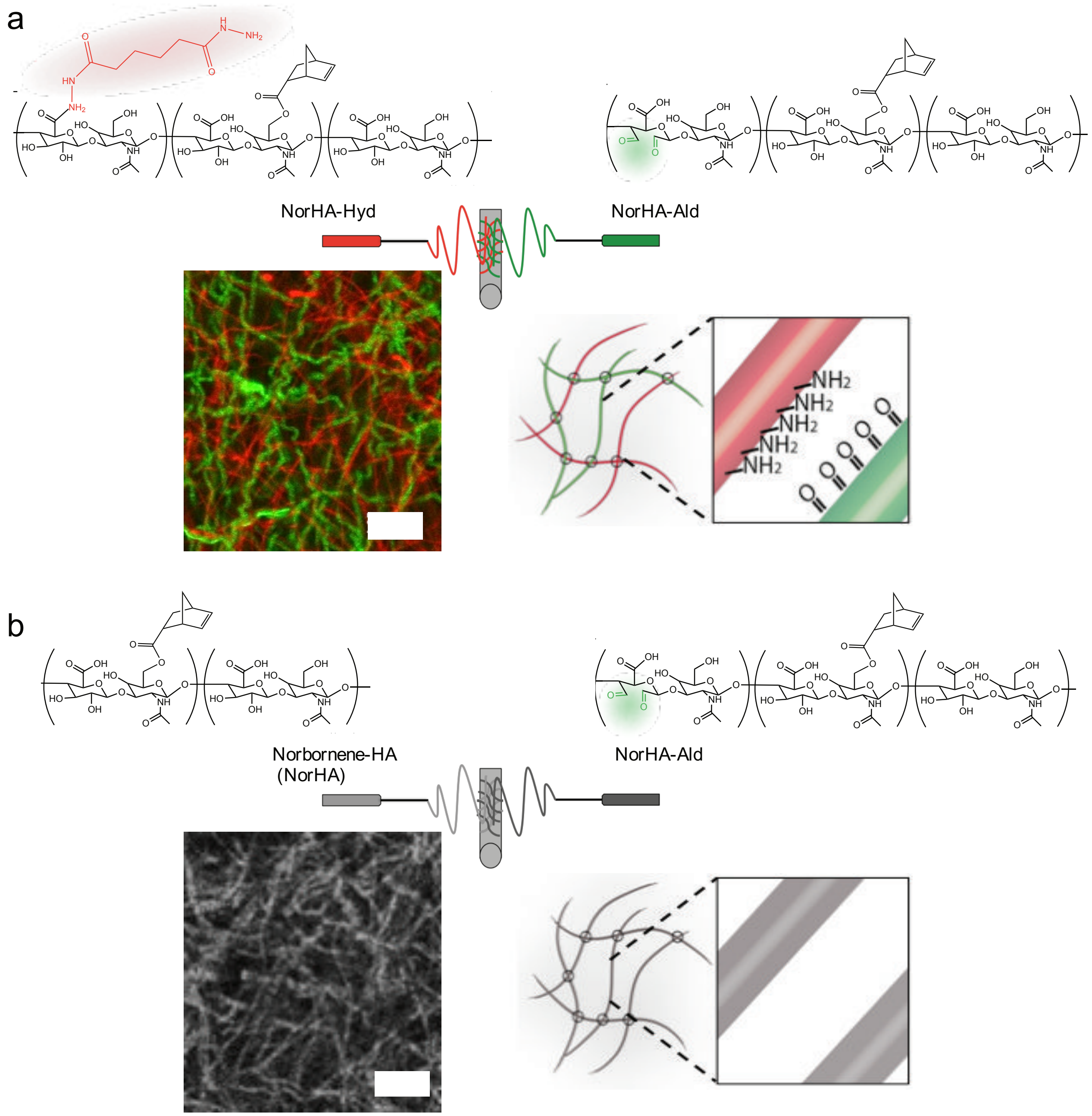

Figure S3. Fabrication of adhesive and non-adhesive multi-fibrous hydrogel networks. (a) Adhesive fibers were fabricated with NorHA-Hyd (red) and NorHA-Ald (green) via multi-fiber electrospinning. Image shows representative confocal microscopy of hydrated adhesive fibrous hydrogel network. (b) Non-adhesive fibers were fabricated with NorHA and NorHA-Ald via multi-fiber electrospinning. Image shows representative confocal microscopy (converted to gray-scale) of hydrated non-adhesive fibrous hydrogel network. Scale bar is 10µm.

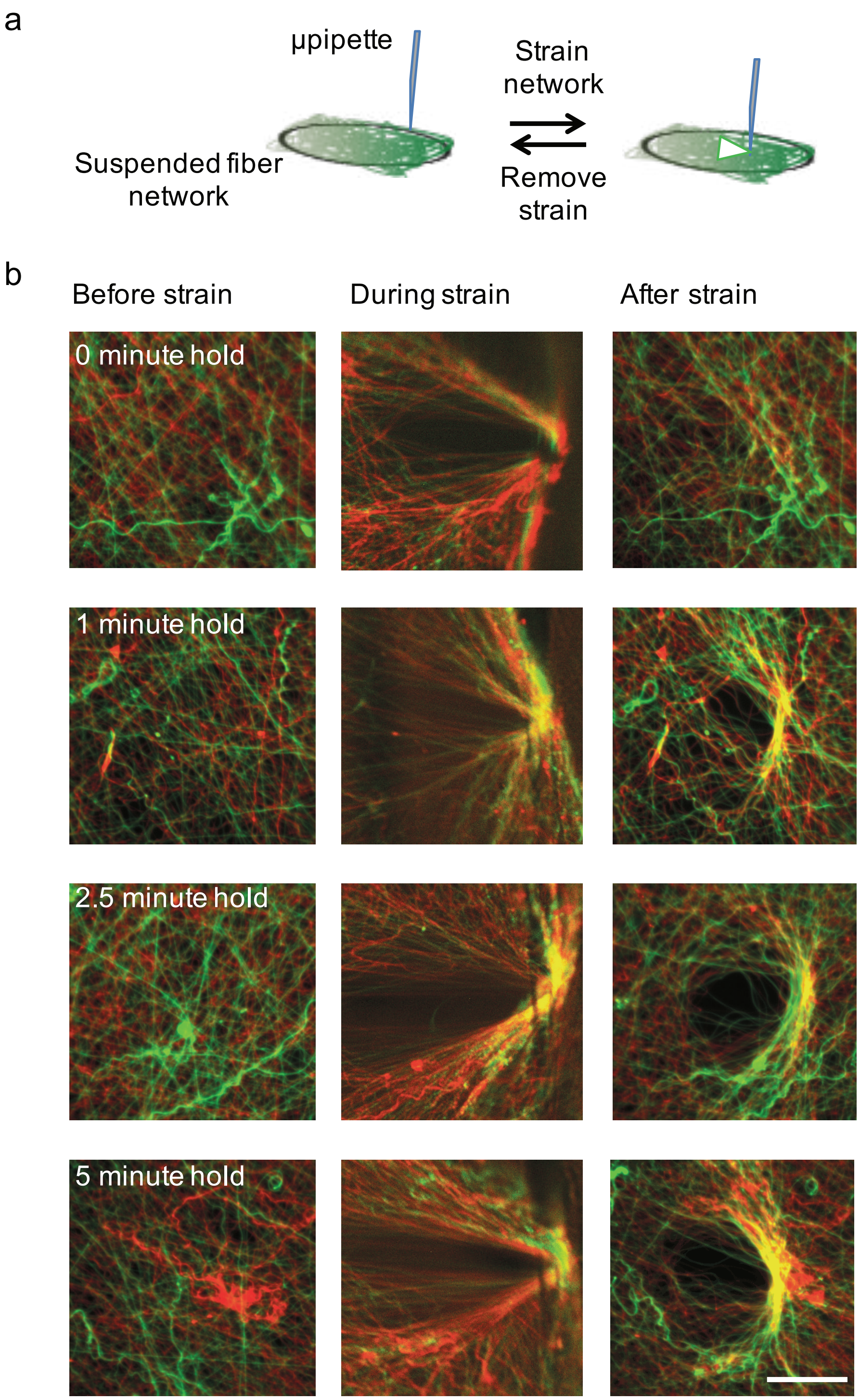

Figure S4. Design and manipulation of suspended fibrous hydrogel networks to assess inter-fiber adhesion and kinetics. (a) Schematic of technique used where suspended fibers are compressed with a micropipette (~5µm diameter bore size) by inserting the tip into the network and translating the tip 300 µm and holding for various amounts of time and then translating the tip back to its original position. (b) Images of suspended fibers before, during, and after compressive strain through manipulator for various holding times to assess the influence of this time on inter-fiber adhesion and plastic deformation. Scale bar is 50µm.

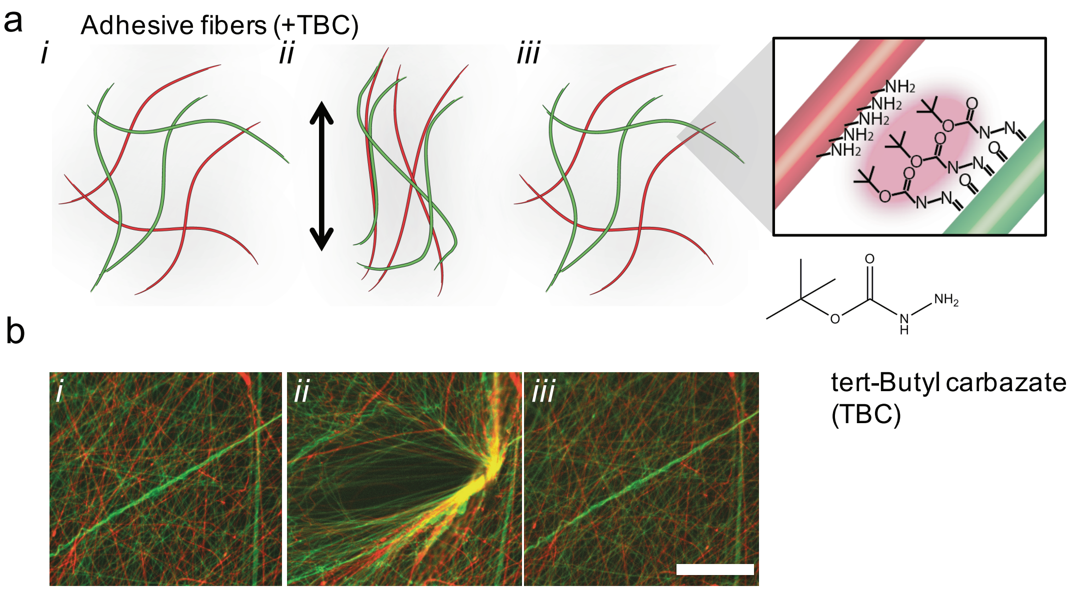

Figure S5. Blocking hydrazone bond formation prevents inter-fiber adhesion. (a) Aldehyde groups on adhesive fibers have a high affinity for tert-butyl carbazate (TBC). Hydrating fibers in a solution of TBC (50mM) leads to deactivation of aldehydes preventing adhesion between fibers when in contact under strain. (b) Representative images of adhesive fibers (I) before, (II) during, and (III) after compression with manipulator after hydration in TBC. Scale bar is 100µm.

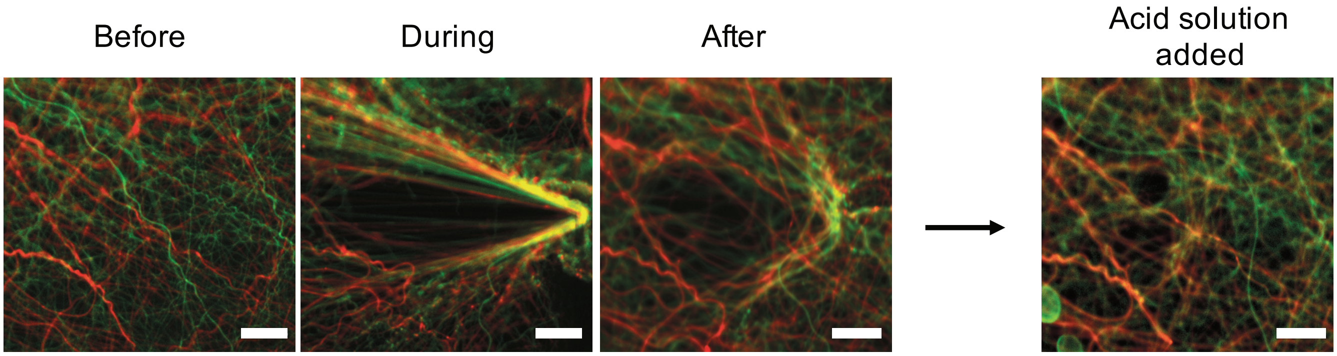

Figure S6. Disrupting hydrazone bonds by lowering pH. Suspended fibers were plastically compressed using a micromanipulator, and then plastic remodeling was rapidly disrupted by lowering pH with acetate buffer (pH 4.3). Scale bar is 50µm.

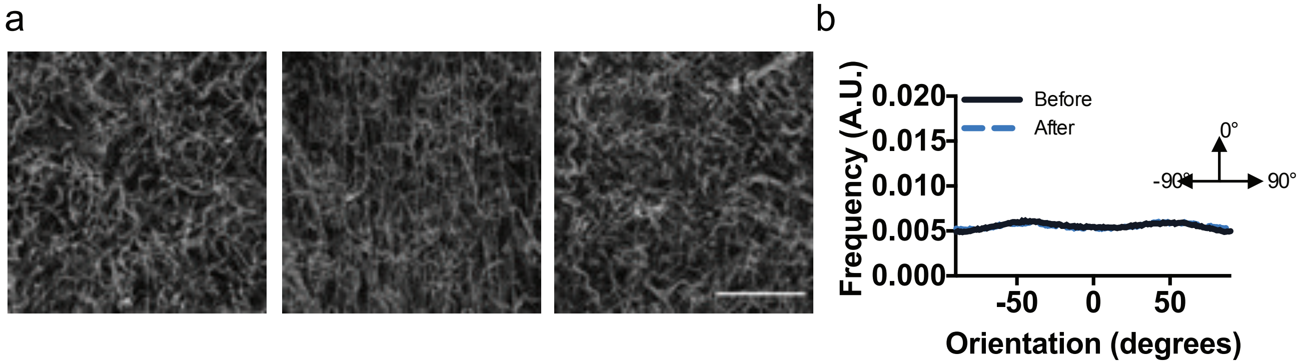

Figure S7. Non-adhesive fibers lack strain responsive changes in fiber orientation. (a) Representative confocal images of non-adhesive fibers before (left), during (middle) and after removing strain (right). (b) Orientation of fibers before and after straining and holding for 1 hour before removing strain. Scale bar is 50 µm.

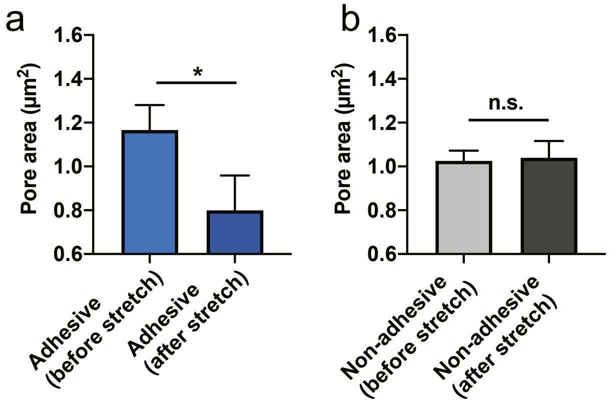

Figure S8. Effects of strain on porosity in adhesive and non-adhesive fibers. Images from the experiments described in the text where fibrous hydrogels were strained, held, and then strain was removed, were used to assess changes in porosity due to straining (a) adhesive and (b) non-adhesive fibrous hydrogels. * represents $p \leq 0.05$.

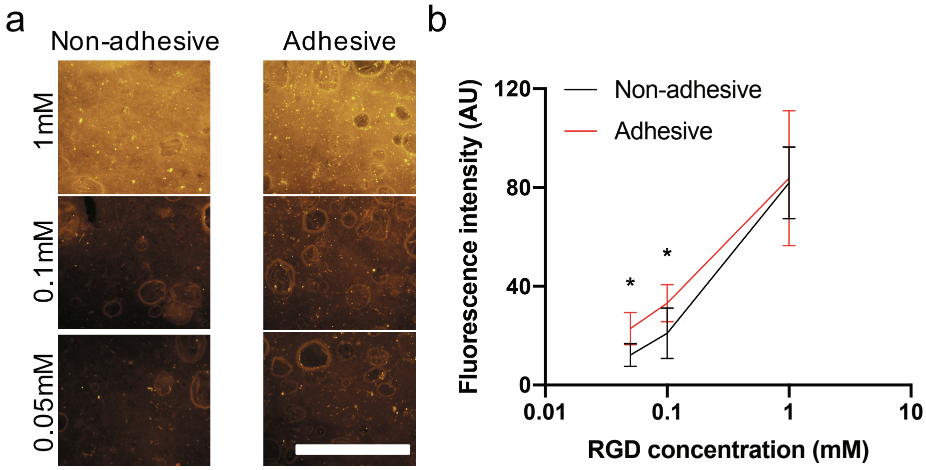

Figure S9. Characterization of RGD conjugation to fibrous hydrogel networks. (a) Rhodamine B-RGD peptides (0.05mM-1mM) and photoinitiator were incubated with non-adhesive (left) or adhesive (right) fibrous hydrogel networks, and conjugated to norbornene groups on HA through a photoinitiated thiol-ene reaction (5 mW/cm^2, 5 min). (b) Fluorescence intensity was quantified and used as a marker of RGD labeling efficiency. Scale is 500 µm. * represents $p \leq 0.05$

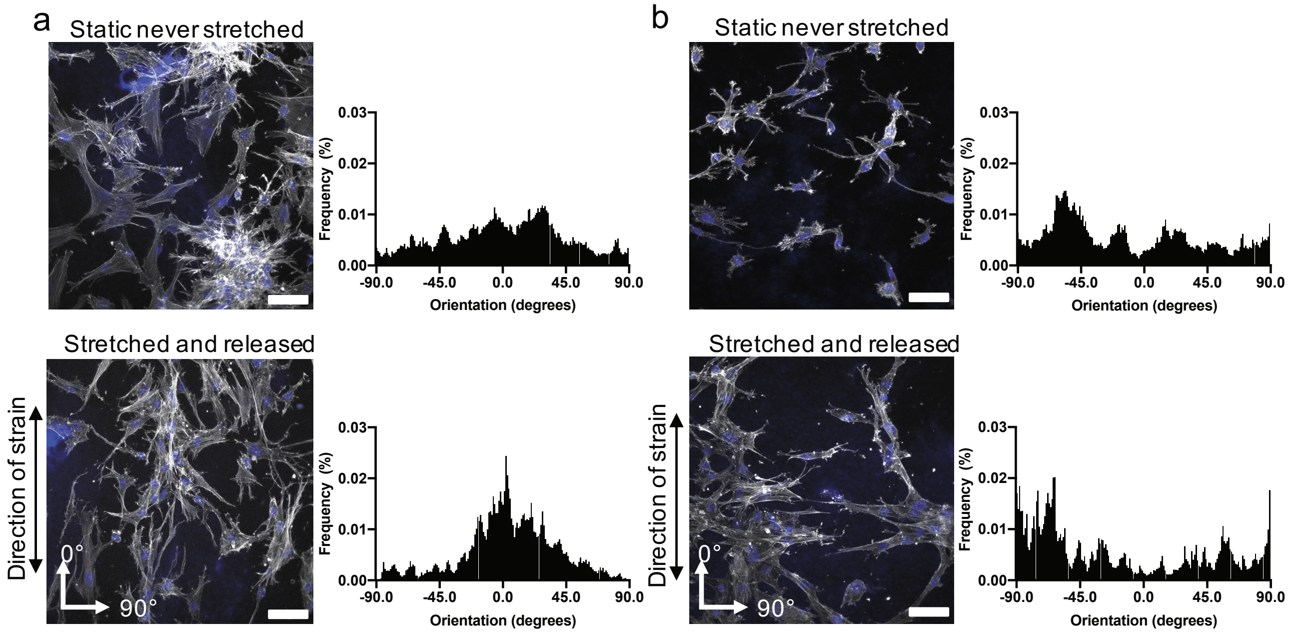

Figure S10. Stretching and releasing of cell laden fibrous hydrogels. (a) Adhesive and (b) non-adhesive fibrous hydrogels were conjugated with RGD, and then seeded with MSCs. After 4 hours, substrates were either (top) cultured statically for 24 hours without stretching or (bottom) strained to 50%, held for 1 hour, and then the strain was released and cells were cultured for 24 hours. After 24 hours, cultures were fixed, stained for f-actin and DNA, and imaged using a confocal microscope. Cell orientation was quantified as actin orientation measured using OrientationJ in FIJI. Scale bar is 100 µm.

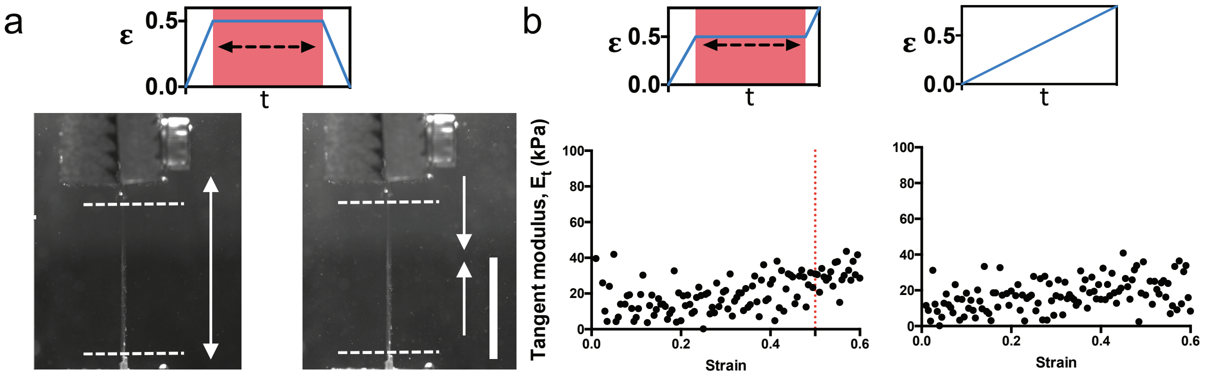

Figure S11. Non-adhesive fibers lack strain responsive changes in mechanical properties. (a) Non-adhesive fibers were strained to 50% strain, held for 10 minutes and then returned to their original length and imaged from the side before (left) and after (right) straining and holding. Scale bar is 15mm. (b) Representative plots of tangent stiffness from non-adhesive fibers strained with holding at 50% strain (right) or without holding (left).

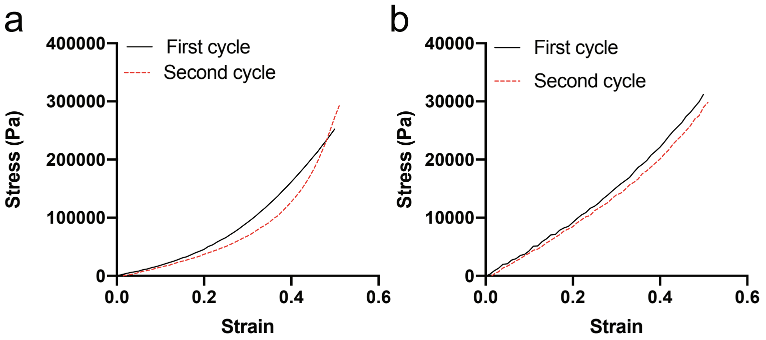

Figure S12. Cyclic loading of fibrous hydrogels. (a) Adhesive and (b) non-adhesive fibrous hydrogels were loaded in tension to 50% strain, unloaded, and then loaded again to 50% strain.

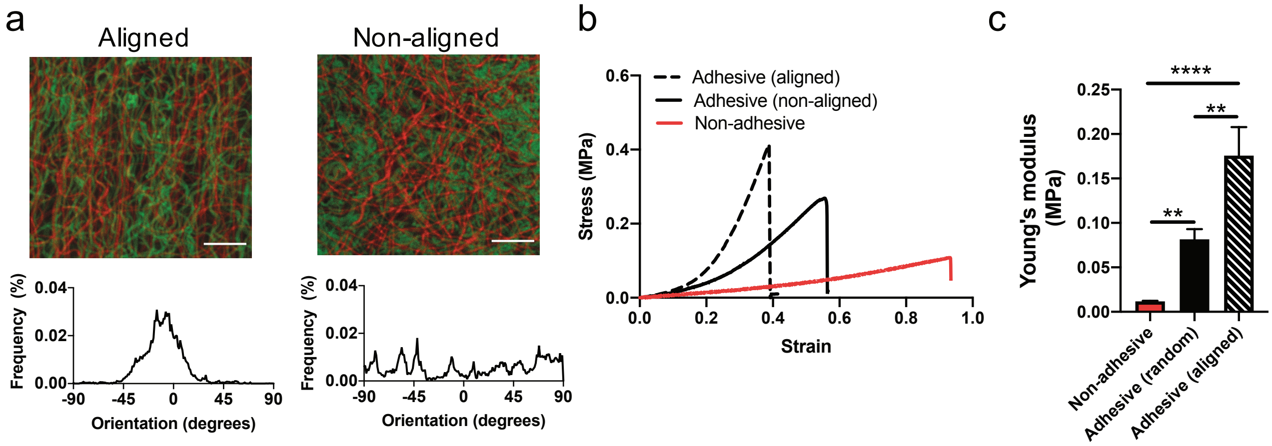

Figure S13. Effects of microscale anisotropy and hydrazone bonds on fibrous hydrogel mechanics. (a) Aligned and non-aligned adhesive fibers (top) were fabricated and alignment was quantified from images (bottom). (b) Stress-strain curves of adhesive aligned (dotted black), adhesive non-aligned (solid black), and non-adhesive fibers (red) strained in tension to failure, and (c) Young's moduli calculated at 5-15% strain. Scale bar is 20 µm. **,**** represent $p \leq 0.01$, $p \leq 0.0001$.

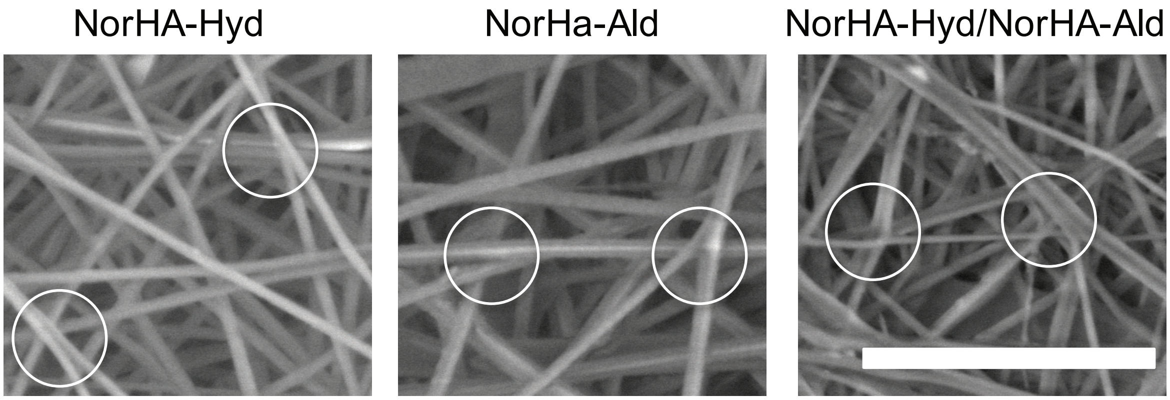

Figure S14. Scanning electron microscopy (SEM) characterization of fiber topography and inter-fiber welding. (a) NorHA-Hyd, (b) NorHA-Ald, and (c) a mixed population of NorHA-Hyd and NorHA-Ald were electrospun and photocrosslinked prior to SEM imaging in the non-hydrated state. White circles outline areas of inter-fiber welding. Scale bar is 5µm.

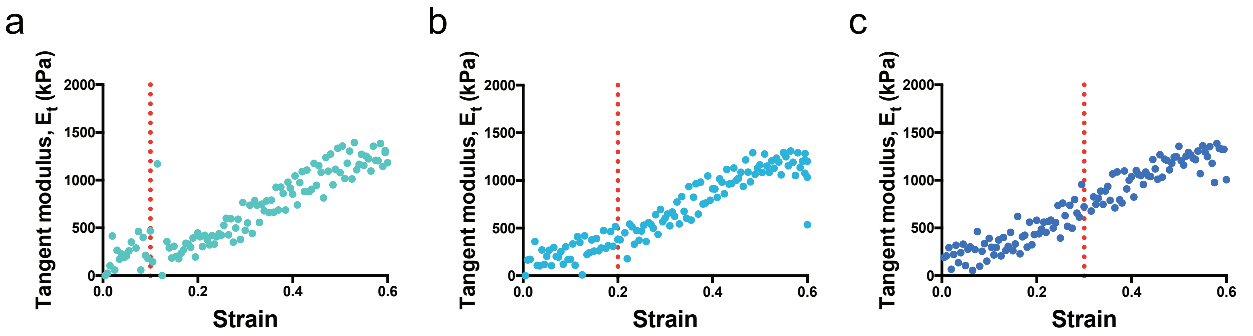

Figure S15. Adhesive fibers do not undergo strain-induced stiffening at strains below 50%. Representative tangent modulus plots of adhesive fibers strained with holding for 20 minutes at (a) 10 %, (b) 20%, or (c) 30% strain. Red line indicates strain where holding occurred.

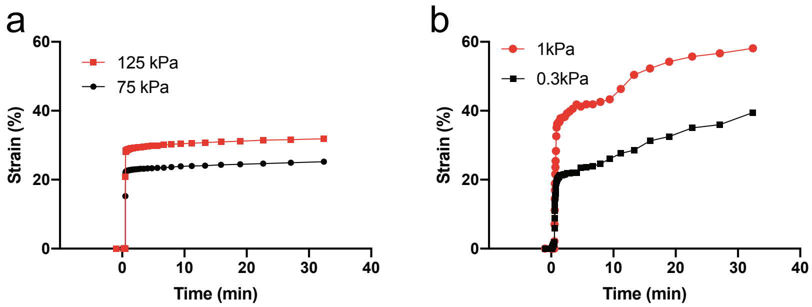

Figure S16. Extended creep testing of adhesive and non-adhesive fibrous hydrogels. Materials were hydrated, equilibrated at room temperature, and then exposed to creep testing for 30 minutes. (a) adhesive fibers were exposed to 75kPa (black) or 125kPa (red) of tensile stress, while (b) non-adhesive fibers were exposed to 0.3kPa (black) or 1kPa (red) of tensile stress.

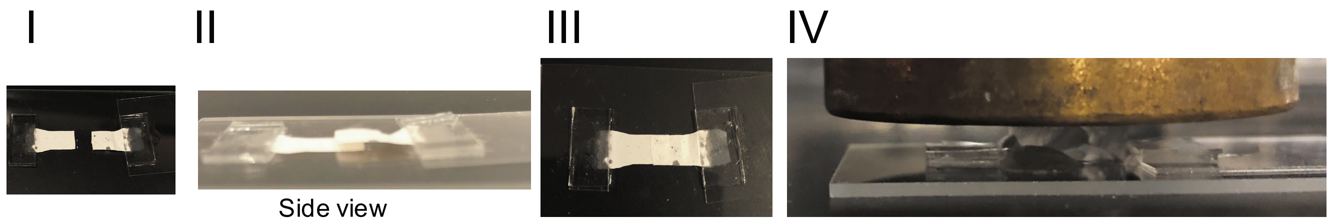

Figure S17. Sample preparation and treatment for self-adhesion test. (I) Dry fiber mats were cut and (II) overlapped and (III) compressed together and (IV) hydrated under compression for 20 minutes.

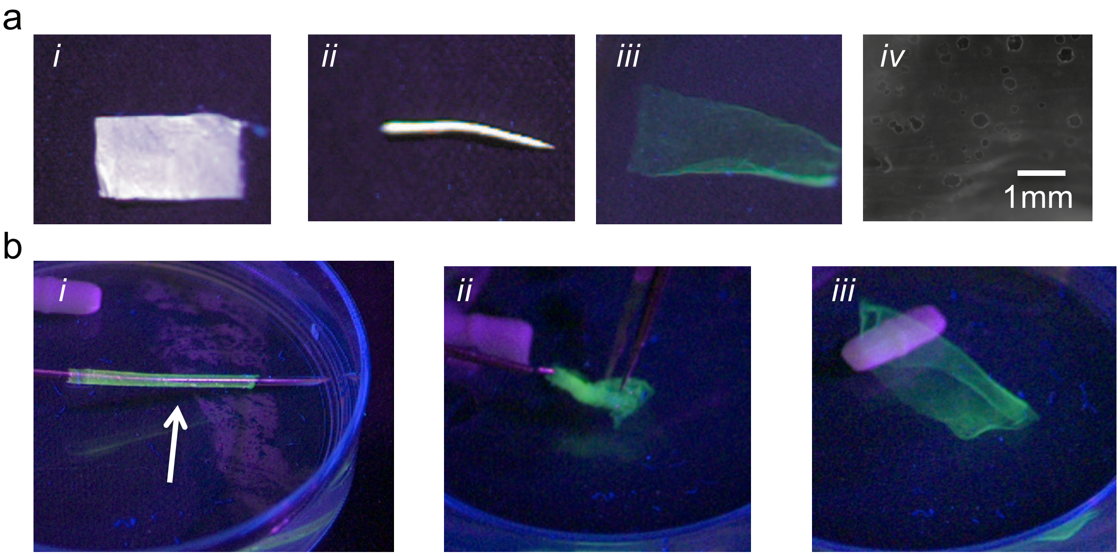

Figure S18. Non-adhesive fibers do not retain macroscale shape with mechanical agitation. (a) (I) Non-adhesive fiber mats were (II) twisted into helical structure and (III) hydrated with mechanical agitation. (IV) Fluorescent micrograph of fiber mat after agitation. (b) Non-adhesive fibers were (I) wrapped around an 18 G needle and hydrated, and then (II) removed from the needle with forceps and (III) mechanically agitated with a stir bar.

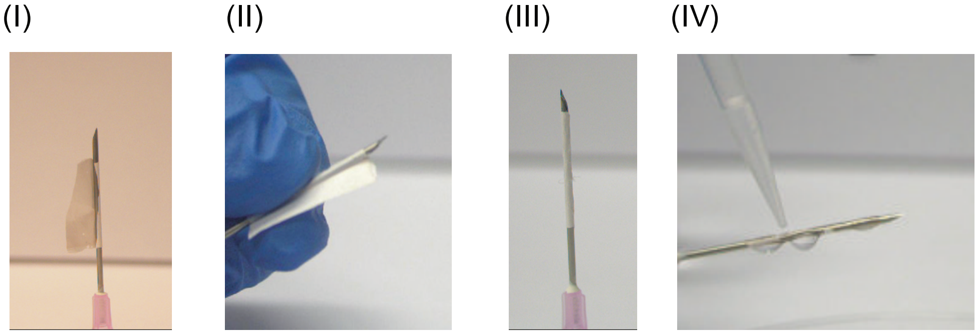

Figure S19. Process for fabricating lumen structure with fiber mats. (I) Fiber mats are wrapped around an 18 G needle and then (II) manually rolled around the needle until (III) the entire mat is completely wrapped around the needle and then (IV) hydrated.

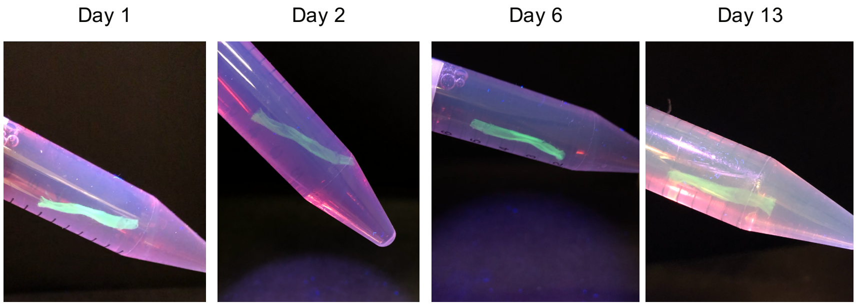

Figure S20. Stability of adhesive fiber macroscale structure over time in cell culture media. Adhesive fibers were formed into a lumen structure, as described in the text, and then transferred into cell culture media and incubated at 37°C for indicated time. Image shows same lumen structure over time.

Supplementary Figures

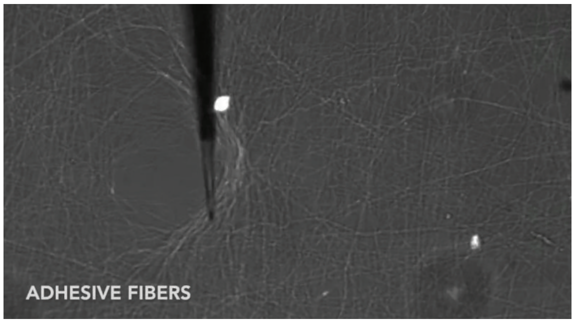

Video S1. Microscale compression of suspended fibrous hydrogel networks, including adhesive fibers, non-adhesive fibers, and adhesive fibers treated with tert-butyl carbazate.

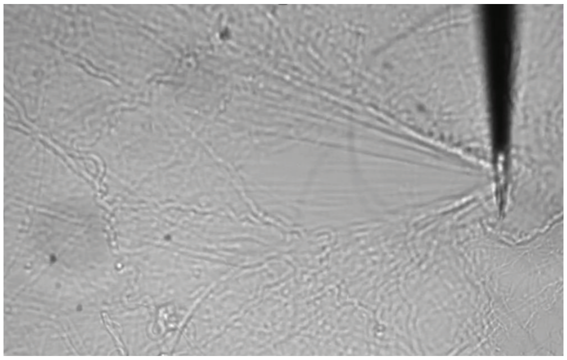

Video S2. Microscale compression of suspended fibrous hydrogel networks of adhesive fibers, including disruption of adhesion (via hydrazone bonds) with acetate solution at pH 4.3.

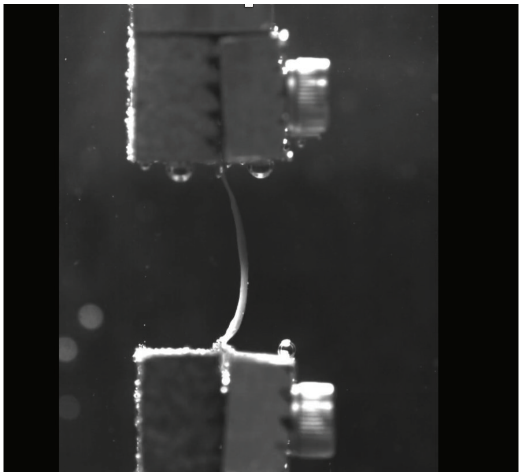

Video S3. Side view of tensile tested fibrous hydrogel networks, including adhesive and non-adhesive fibers.

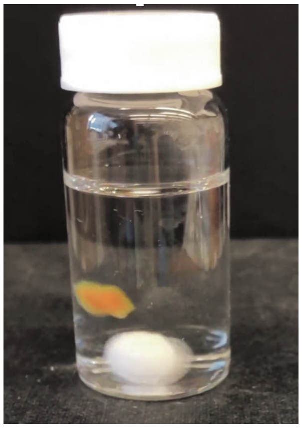

Video S4. Agitation of layered adhesive fibrous hydrogel constructs.

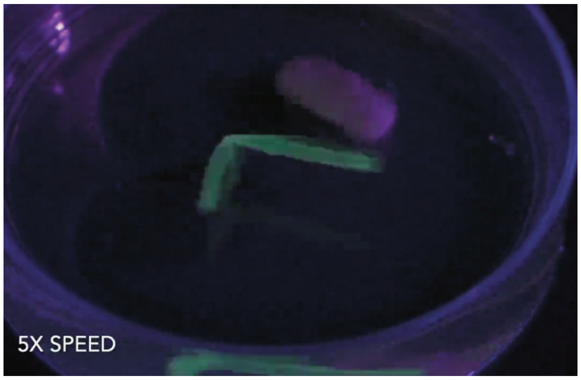

Video S5. Fabrication and agitation of lumen structures from both adhesive and non-adhesive fibrous hydrogel networks.

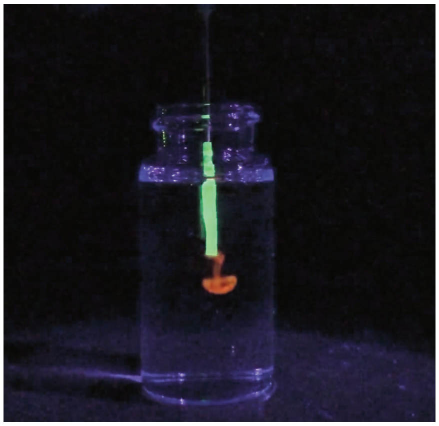

Video S6. Extrusion of rhodamine-labeled dextran through a lumen structure fabricated from adhesive fibrous hydrogel networks.

References

[1] A. S. Abhilash, B. M. Baker, B. Trappmann, C. S. Chen, V. B. Shenoy, *Biophys. J.* **2014**, *107*, 1829.

[2] E. Ban, J. M. Franklin, S. Nam, L. R. Smith, H. Wang, R. G. Wells, O. Chaudhuri, J. T. Liphardt, and V. B. Shenoy, Biophys. J. **114**, 450 (2018).

[3] T. J. R. Hughes, *The Finite Element Method: Linear Static and Dynamic Finite Element Analysis* (Courier Corporation, 2012).

[4] E. Riks, Int. J. Solids Struct. **15**, 529 (1979).

[5] Hibbett, Karlsson, and Sorensen, *ABAQUS/Standard: User's Manual* (Hibbitt, Karlsson & Sorensen, 1998).

[6] E. Ban, H. Wang, J. M. Franklin, J. T. Liphardt, P. A. Janmey, and V. B. Shenoy, Proc. Natl. Acad. Sci. 201815659 (2019).

[7] B. P. Purcell, D. Lobb, M. B. Charati, S. M. Dorsey, R. J. Wade, K. N. Zellars, H. Doviak, S. Pettaway, C. B. Logdon, J. A. Shuman, P. D. Freels, J. H. Gorman, R. C. Gorman, F. G. Spinale, J. A. Burdick, *Nat. Mater.* **2014**, *13*, 653.